JCTC Journal of Chemical Theory and Computation

Article

pubs.acs.org/JCTC

Transferability and Nonbond Functional Form of Coarse Grained Force Field – Tested on Linear Alkanes

Fenglei Cao[†] and Huai Sun*[,†,‡]

[†]School of Chemistry and Chemical Engineering and Key Laboratory of Scientific and Engineering Computing of Ministry of Education, Shanghai Jiao Tong University, Shanghai 200240, China

[‡]State Key Laboratory of Inorganic Synthesis & Preparative Chemistry, College of Chemistry, Jilin University, Changchun, Jilin 130012, China

Supporting Information

ABSTRACT: Whether or not a coarse grained force field (CGFF) can be made to be transferrable is an important question to be addressed. By comparing potential energy with potential of mean force (PMF) of a molecular dimer, we proposed to use a free energy function (FE-12-6) with the parameters in entropic and energetic terms explicitly to represent the nonbond interactions in CGFF. Although the FE-12-6 function cannot accurately describe the PMF curves, a cancelation of short radii and strong repulsion makes the function a good approximation. For nonpolar molecules represented by linear alkanes, FE-12-6 is demonstrated to be highly effective in representing the nonbond interactions in CGFF. The force field parameters are well transferrable among different alkane molecules, in different thermodynamic states and for predicting various thermodynamic properties including heats of vaporization, vapor–liquid-equilibrium coexistence curves, surface tensions, and liquid densities.

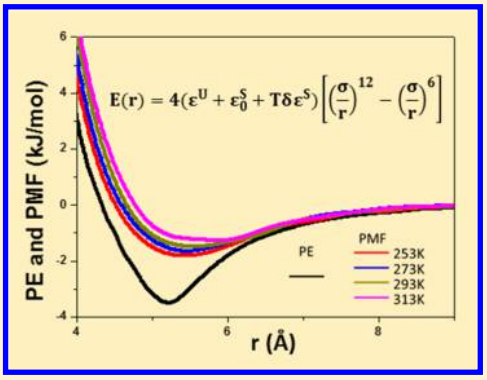

I. INTRODUCTION

The coarse grained force field (CGFF) provides computational and conceptual advantages over atom-specific force field.[1−6] Significant efforts have been devoted to parametrizations, either from data of atom-specific simulations (bottom-up)[7−17] or from data of experimental measurements (top-down).[18−26] It is well-known that the predictive power of a force field depends on the transferability of its parameters. Generally speaking, parameters can be used in different molecules consisting of the same functional groups because of the transferability of chemical groups.[18−22] To use the same force field in different state points (e.g., temperatures) is more difficult to achieve.[18,19,27−30] Furthermore, to use the same force field to predict different physical properties is perhaps the most difficult task as force fields are generally derived with limited scope of application.[5,22] Overall, whether a CGFF can be made to be transferrable is still an unresolved question.[19,22,27−32]

The bottom-up approach constructs a CGFF as a systematic approximation to the many-body potential of mean force (PMF) of an all-atom (AA) model. Because PMF is too complex to be represented by simple analytical function, tabular function is used for this type of CGFF. While the PMF can be accurately represented, the transferability depends on the underlying PMF, which necessarily relies on mapping rule, molecular system and thermodynamic state point.[33] This problem is evident by the fact that the transferability of CGFF derived from PMF depends on mapping rules[27] and rescaling or interpolating of temperatures.[27−30]

The top-down approach determines the interactions between CG sites by numerically fitting experimental data to analytic potential functions.[5] Depending on the functional forms and the amount of data to fit, various degrees of transferability have been achieved. The Martini force field[18] is optimized to reproduce the free energies of hydration and partition coefficients at constant temperature and pressure commonly found in biological systems; the transferability in different state points and physical properties are not rigorously tested. The SDK force field[19,20] has been shown transferable in predicting various properties relevant to surfactant normally at ambient temperatures. The TraPPE-CG force field[22] exhibits reasonably good transferability in temperatures and properties for alkane molecules. The SAFT-γ force field[23−26] with more complicated Mie function[34] and polynomial expansion in temperature[26] demonstrates good transferability over a wide range of state points and physical properties.

Although more parameters can be helpful for making a force field more accurate, it is the underlying functional form that fundamentally determines the transferability of a force field. The functional form should represent the complex energy hypersurfaces with as few adjustable parameters as possible, so that a small number (more than the number of the adjustable parameters) of training data is sufficient to determine the parameters. Although a "correct" functional form may not exist in the empirical force field, a good approximation may be made.

Received: June 18, 2015
Published: September 3, 2015

DOI: 10.1021/acs.jctc.5b00573
J. Chem. Theory Comput. 2015, 11, 4760−4769

For example, a combination of the Lennard-Jones (LJ) function for describing van der Waals interactions and the columbic function for describing electrostatic interactions is reasonably accurate to represent the intermolecular interactions at the atomistic level, which is demonstrated by the fact that AA or united-atom (UA) force fields can be parametrized to be transferrable in a broad range of state points and molecules and for predicting different properties.[35−37] What functional form is suitable for describing the intermolecular interactions at the CG bead level is a question to be addressed.

The PMF between CG beads calculated at the AA level can be decomposed to energetic and entropic contributions.[38−40] Taking this perspective, we seek a formula that explicitly includes the energetic and entropic contributions to describe the interactions between CG beads. Since the nonbond parameters are the most sensitive for predicting physical properties of condensed matters while the intrabead parameters that determine the molecular structures and conformations are not too difficult to derive, we constructed our work based on existing SDK[19] force field and focused on the nonbond interactions only. As the first step, we considered the nonpolar molecules with van der Waals (VDW) terms only. Using linear alkane as an example, we found that the classical LJ-12-6 type function with parameters separated to energetic and entropic contributions is a good approximation. We tested this free energy nonbond function (FE-12-6) by fitting to various liquid properties including heats of vaporization (HOV), vapor liquid equilibrium (VLE) coexistence curves, surface tensions (γ), and P-V-T equations of state. The amount of data is sufficient to determine the adjustable parameters and to validate the proposed functional form. The results are encouraging, the force field exhibits high transferability in all molecules considered (including the testing set), in a broad range of state points and for different properties.

This paper is organized as follows: In Section II, we present the simulation protocols that are used in this work. Section III is used to explain and discuss how the energetic and entropic terms in nonbond interactions are derived. Section IV is for the parametrization and validation; we explain how the parameters are derived and validated and discuss the physics meaning of the derived parameters. Finally, we make a conclusion of this work in Section V.

II. SIMULATION METHODS

The simulations at the AA level were carried out using in-house developed TEAM force field. The PMF[41] was calculated using umbrella samplings with a harmonic potential. The umbrella window spacing was 0.5 Å to ensure sufficient overlaps between any two windows. In each window, 2 ns of NVT molecular dynamics (MD) simulation was performed to evaluate the potential energies. The weighted histogram analysis method (WHAM)[42,43] was used for evaluating the averaged PMF values. These calculations were conducted using the GROMACS software package (version 4.0.3).[44]

In the SDK[19] force field, the linear alkane molecules are represented by the 3 + 2 mapping rule using three bead types: C2E (CH_3CH_2-), C3E ($CH_3CH_2CH_2$-), and C3M ($-CH_2CH_2CH_2$-). For examples, *n*-hexane is represented by a linear chain of two C3E beads, and *n*-undecane is modeled as a linear chain of one C2E bead, two C3M beads, and one C3E bead. The intramolecular interactions consist of bond stretching (1−2), angle bending (1−2−3), and a correction term for 1−3 interaction. The beads separated by more than two bonds in the same molecule or between different molecules interact via the nonbond force, which is described by the VDW term only. The VDW term is represented by a LJ function (12−4 or 9−6).[19] More information about the force field is given in the Supporting Information (SI).

The Gibbs Ensemble Monte Carlo (GEMC)[45] simulations in the canonical (NVT) ensemble were conducted to calculate the VLE coexistence curves. Two boxes representing the vapor and liquid phases with a total of 600 molecules were used in these simulations. The GEMC moves included swapping molecules between the vapor and liquid boxes, volume exchanges, and translations and rotations of molecules in each of the two boxes. Each of the GEMC simulations included 3×10^7 steps for equilibration and 7×10^7 steps for data collection. From the coexistence curves, the critical temperature T_c was estimated using the scaling law

$$\rho_{liq} - \rho_{vap} = B(T - T_c)^{0.325} \tag{1}$$

where ρ_{liq} and ρ_{vap} are the saturated liquid and vapor densities. The critical density ρ_c was estimated using the law of rectilinear diameters

$$\frac{1}{2}(\rho_{liq} + \rho_{vap}) = \rho_c + A(T - T_c) \tag{2}$$

where A and B are correlation parameters.[22] The GEMC simulations were carried out using Towhee 7.0.3 programs.[46]

The isobar-isotherm ensemble (NPT) MD simulations were conducted to calculate liquid densities. The trajectories of simulation were sampled every 1000 steps to calculate HOV by

$$\Delta H_v = -E_{liquid,inter} + RT \tag{3}$$

where $E_{liquid,inter}$ is the cohesion energy of liquid. The NVT MD simulation was carried out on a slab model to calculate the surface tension (γ) from pressure tensors

$$\gamma = \frac{L_z}{2}\left\{P_{zz} - \frac{P_{xx} + P_{yy}}{2}\right\} \tag{4}$$

where the factor of 1/2 is included to account for the two interfaces in the slab model, P_{ij} is the component of the averaged pressure tensor, and L_z is the length of Z-direction of simulation box. The simulation boxes were $10 \times 10 \times 10$ nm for the bulk models and $10 \times 10 \times 20$ nm for the slab models. The slab model was created by extending the cubic model in the z-direction by adding 10 nm vacuum. The equilibration period included 2 ns with time step of 2 fs and 5 ns with time step of 10 fs. The production period consisted of 10 ns simulation with time step of 10 fs. The temperature and pressure were controlled using the Nose-Hoover method with a coupling constant of 100 steps. The initial configurations were generated by using the Packmol program,[47] and the MD simulations were performed using the Lammps program.[48]

In all CG simulations, the nonbond interactions were evaluated using a fixed cutoff (r_{cutoff}) of 20 Å, which is greater than 4σ[23] as the largest σ in the beads is 4.6 Å. The block-average method[49] was used to estimate uncertainties of calculated properties.

For comparison, we calculated properties using TraPP-CG,[22] SDK,[19] and Martini[18] force fields. Due to the differences in mapping rules, the TraPPE-CG model was used for calculations on hexane, nonane, and dodecane only; the Martini model was used for octane and dodecane only. In the Martini model, the

DOI: 10.1021/acs.jctc.5b00573
J. Chem. Theory Comput. 2015, 11, 4760−4769

mass was fixed at 72.00 for each bead during the simulation[18] and then replaced by the real mass to calculate densities.

III. FREE ENERGY NONBOND FUNCTION

Figure 1 shows the calculated potential energy (PE) and PMF curves as the distance between the centers of mass of two

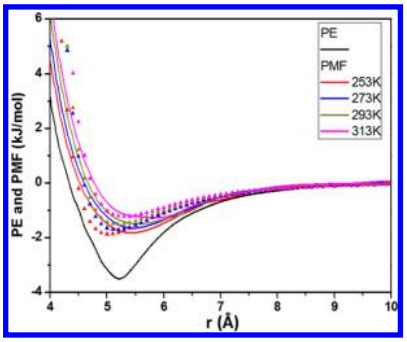

Figure 1. Potential energy (PE) and potential of mean force (PMF) at 253, 273, 293, and 313 K for propane−propane dimer. FE-12-6 function with $\varepsilon^U + \varepsilon_0^S$ = 3.6 kJ/mol, $\delta\varepsilon$ = −0.007 kJ/mol/K, $\sigma^U + \sigma_0^S$ = 4.6 Å, $\delta\sigma$ = 0.0008 Å/K are shown by dots.

propane molecules. The PMF curves, calculated at 253, 273, 283, and 313 K, are shifted up and right from the PE curve, and the differences increase as the temperature increases. The reduction in the well-depth is due to that part of the potential energy is converted to intramolecular entropy, and the increased radii represents that the effective size of the molecule is increased, both due to intramolecular vibrations.

The PMF curves in Figure 1 can be approximated by a LJ-12-6 type function

$$E(r) = \varepsilon(T)\left[\left(\frac{\sigma(T)}{r}\right)^{12} - \left(\frac{\sigma(T)}{r}\right)^{6}\right] \quad (5)$$

where the coefficients are temperature dependent:

$$\varepsilon(T) = \varepsilon^U + \varepsilon^S(T) = \varepsilon^U + \varepsilon_0^S + \mathrm{T}\,\delta\varepsilon^S \quad (6)$$

$$\sigma(T) = \sigma^U + \sigma^S(T) = \sigma^U + \sigma_0^S + \mathrm{T}\,\delta\sigma^S \quad (7)$$

Both well-depth parameter $\varepsilon(T)$ and radii parameter $\sigma(T)$ are written as the sum of energetic (ε^U, σ^U) and entropic ($\varepsilon^S(T)$, $\sigma^S(T)$) terms. The entropic terms are further expressed as linear functions of temperature (ε_0^S + T $\delta\varepsilon^S$) and (σ_0^S + T $\delta\sigma^S$), where ε_0^S and σ_0^S may be interpreted as the residual entropic contributions at 0 K. To distinguish the function given in eq 5 from a normal LJ-12-6 function, we refer to it as free energy 12-6 function, abbreviated as the FE-12-6 function. As the intrabead terms are taken from SDK, we denote the new force field as SDK/FE-12-6 in this work.

Using the PMF data, we obtained the parameters of the FE-12-6 function as follows:

$$\varepsilon^U + \varepsilon_0^S = 3.6\ \mathrm{kJ/mol}, \quad \delta\varepsilon^S = -0.007\ \mathrm{kJ/mol/K}$$

$$\sigma^U + \sigma_0^S = 4.6\ \text{Å}, \quad \delta\sigma^S = 0.0008\ \text{Å/K}$$

The FE-12-6 curves using above parameters are compared with the PMF curves in Figure 1. The FE-12-6 function matches the radii and the well depth of PMF, but the repulsion part is too steep and the minimum energy radii is too short by about 0.5 Å. Overall, the strong repulsion is compensated by the short radii so that the total interaction strength would be about the same in comparison with the true PMF value. We tested various functions and found that the Buckingham and LJ-4-6 functions yield better fits of the PMF curves (shown in Figures S2 and S3 in the SI). However, both functions are unstable at short distances and not popular in simulation software packages. More importantly, the FE-12-6 function appears to be a good approximation for the molecules considered in this work. Considering all of these factors, we choose to use the FE-12-6 function.

The two-body PMF used for deriving the FE-12-6 function exhibits monotonic curve in the attractive region, which is different from the multibody PMF curves with structural features in the attractive region. To show that the liquid structures can be approximated by the pairwise FE-12-6 function, we calculated the radial distribution functions (RDFs) for liquid propane using the CG and AA models. A comparison of the RDFs at different temperatures is shown in Figure 2. Because of the coarse-graining (the propane is

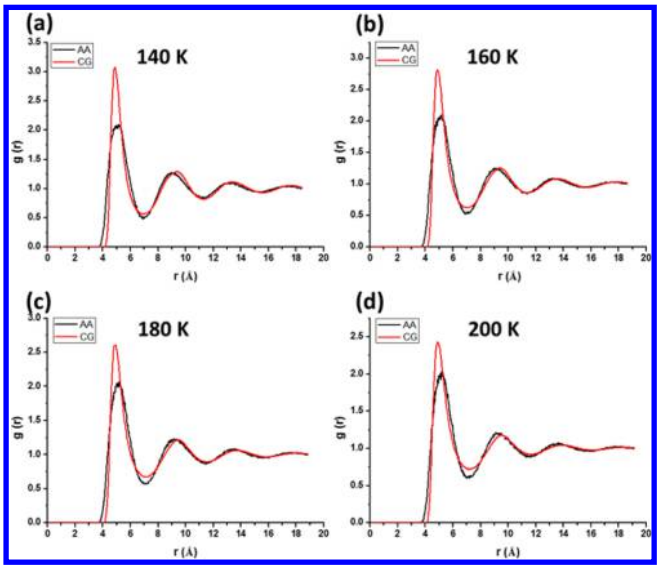

Figure 2. Radial distribution functions of the centers of mass of propane molecules in liquid states, obtained from AA (black line) and CG (red line) models, at various temperatures.

represented by a single bead), there are clearly differences between AA and CG RDFs.[19,22] However, the major characteristics of the AA RDF can be found in the CG RDF. The first peak of CG RDF is higher and narrower than that of AA, but the areas of the first peak representing the coordination numbers (ca. 12) in the first shell are similar. Moreover, the same CG model with the FE-12-6 function generates consistent agreements with the AA model in RDF curves crossing the different temperatures.

IV. PARAMETRIZATION AND VALIDATION

Taking linear alkane which represents the simplest yet the most common functional group as an example, we demonstrate how the FE-12-6 can be used to make a CGFF transferrable in different molecules and state points and for predicting different properties. Using the pairwise convention (no combination law is used), we need to determine 6 pairwise interactions for the 3 bead types; each pairwise term has 6 adjustable parameters. The parametrization procedure includes three steps: 1) determine

DOI: 10.1021/acs.jctc.5b00573
J. Chem. Theory Comput. 2015, 11, 4760−4769

combined parameters $(\varepsilon^U + \varepsilon_0^S)$, $(\sigma^U + \sigma_0^S)$, $\delta\varepsilon^S$, and $\delta\sigma^S$ by fitting the VLE data; 2) separate the energetic contribution form the combined parameters, $(\varepsilon^U + \varepsilon_0^S)$ and $(\sigma^U + \sigma_0^S)$, by fitting the HOV data; 3) validate the parameters by predicting liquid densities and surface tensions.

We started the parametrization from hexane since the molecule contains only one pairwise interaction (C3E-C3E). A total of 40 experimental data in VLE coexistence curves, HOV, liquid densities (ρ_{liq}) and surface tensions (γ), were used to fit the 6 parameters. The combined 4 parameters $(\varepsilon^U + \varepsilon_0^S)$, $\delta\varepsilon^S$, $(\sigma^U + \sigma_0^S)$, and $\delta\sigma^S$ were determined by fitting the VLE data. Figure 3 shows the VLE curves predicted using the optimized

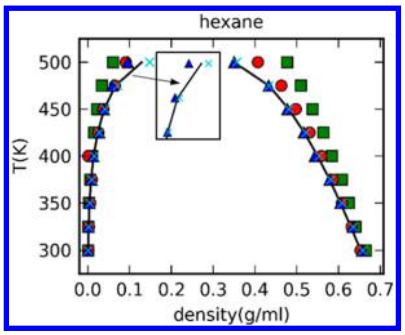

Figure 3. Comparison of the VLE curves for hexane: experimental (solid line) and calculated using TraPPE-CG (red cycle), SDK (green square), and the newly developed SDK/FE-12-6 function with complete parameters (cyan cross) and σ fixed parameters (blue triangle).

FE-12-6 parameters, together with the data calculated using SDK and TraPPE-CG force fields for comparison. The Martini model was not compared because its mapping rule does not support hexane. The SDK force field was developed without consideration of the VLE data;[19] it predicted the curves with large deviation except that at 300 K. The TraPPE-CG force field was optimized by fitting the VLE data at 300, 350, and 400 K;[22] however, it fails at temperatures above 400 K. On the other hand, the FE-12-6 function enables the prediction in excellent agreement with the experimental data at the entire temperature range.

The optimized FE-12-6 parameters in Table 1 show that the temperature-correction parameter of the radii parameter, $\delta\sigma$, is

Table 1. Optimized Nonbond Parameters for C3E-C3E Obtained by Fitting VLE Properties of Hexane Based on the FE-12-6 Function

	$\sigma^U + \sigma_0^S$ (Å)	$\delta\sigma$ (10^{-3} Å/K)	$\varepsilon^U + \varepsilon_0^S$ (kJ/mol)	$\delta\varepsilon$ (J/mol/K)
C3E-C3E	4.5000	0.3	2.4159	−0.5410

fairly small (0.3×10^{-3}). This parameter changes the radii in a temperature range of 200 K by only 0.06 Å, which is about 1.3% of the temperature independent part $(\sigma^U + \sigma_0^S) = 4.5$ Å. It is appealing that the radii parameter could be treated as a constant. We tested this approximation and optimized the radii parameter as a temperature independent variable, and the resulted VLE data are also shown in Figure 3 for comparison. As shown by the inset, only the vapor densities at the high temperatures show small differences. Overall, the fixed radii parameter scheme works fairly well. The average absolute percentage deviations (AAPD = $1/N_p \sum_i^{N_p} |(X_{i,exp} - X_{i,theo})/X_{i,exp}| \times 100$) between the experimental and simulated data are 0.9% and 6.8% for liquid and vapor densities respectively using the temperature independent radii parameter. The agreement is slightly better, with AAPD reduced to 0.6% and 5.2% with the full set of parameters. Because of the small differences, we treat the radii parameter as temperature independent in the rest of this work. The simplified FE-12-6 function is

$$E(r) = (\varepsilon^U + \varepsilon_0^S + \mathrm{T}\,\delta\varepsilon^S)\left[\left(\frac{\sigma}{r}\right)^{12} - \left(\frac{\sigma}{r}\right)^{6}\right] \quad (8)$$

Therefore, there are only four (4) adjustable parameters for each pairwise interaction, and the total number of adjustable parameters is reduced to 24 for linear alkane molecules.

The saturated vapor pressures of liquid hexane obtained from GCMC simulations are compared with the experimental data in Figure 4. The agreement is excellent in the temperature range

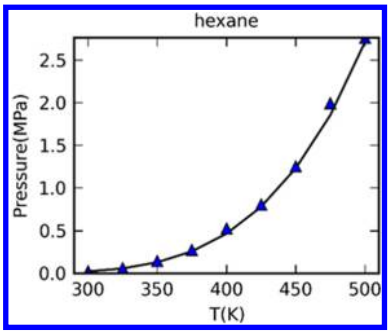

Figure 4. Saturated vapor pressure for hexane: experimental (solid line) and calculated using SDK/FE-12-6 function (blue triangle).

with AAPD of 7.1%. The largest deviation is in the vicinity of the critical region, as expected. Because the vapor pressure is very sensitive to the curvature of interaction function,[50,51] this comparison reinforces that the FE-12-6 is a good approximation in describing the nonbond interactions in CGFF.

The energy contribution in the combined parameters $(\varepsilon^U + \varepsilon_0^S)$ can be obtained by fitting the energetic property HOV. Figure 5 shows the calculated HOV data for liquid hexane from 243.15 to 323.15 K, using the energetic parameters (ε^U, σ) and all FE-12-6 parameters. The results are compared with the experimental data and the data calculated using SDK and TraPPE-CG force fields. The results obtained using the energetic parameters are in good agreement with the

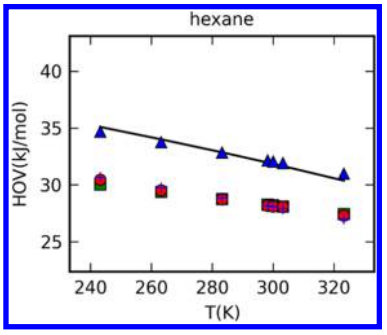

Figure 5. Comparison of HOVs for hexane at different temperatures. The uncertainties of calculated HOV values are lower than 0.2 kJ/mol. The experiment (solid line), SDK/FE-12-6 model with (blue crosses) and without (solid blue triangle) the entropic parameters, TraPPE-CG (red cycle), and SDK models (green square).

DOI: 10.1021/acs.jctc.5b00573
J. Chem. Theory Comput. 2015, 11, 4760−4769

experimental data, with an overall AAPD of 0.6%. It is interesting to note that even though the energetic parameters are temperature independent, the temperature dependent HOV curve can be predicted well. This is due to the fact that the densities are predicted well using the full FE-12-6 function. The predicted densities of liquid hexane at temperatures ranging from 243.15 to 323.15 K under constant (1 atm) pressure are shown in Figure 6, together with the experimental data for

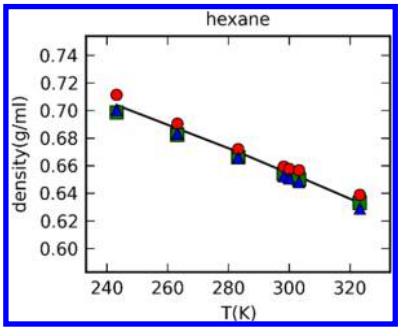

Figure 6. Comparison of the density at 1 atm pressure for liquid hexane. The uncertainties are lower than 0.0002 g/mL. The experiment (solid line), SDK/FE-12-6 (solid blue triangle), TraPPE-CG (red cycle), and SDK (green square) models.

comparison. The FE-12-6 parameters as well as the SDK and TraPPE-CG models reproduce the bulk liquid densities very well. The AAPDs are 0.6%, 0.3%, and 1.2% for this work and SDK and TraPPE-CG models, respectively. However, with the full FE-12-6 parameters, the HOV values are underestimated by 4−5 kcal/mol systematically. Similar underestimates are observed for the SDK and TraPPE-CG models.

The calculated surface tensions of hexane at different temperatures are compared with the experimental data in Figure 7. The SDK model yields accurate predictions for

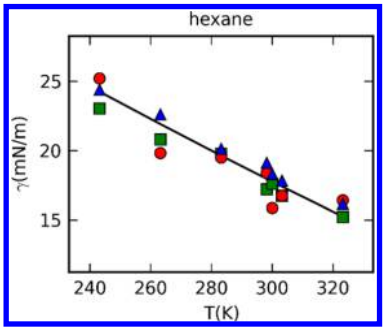

Figure 7. Comparison of the surface tensions for liquid hexane. The uncertainties are lower than 2.5 mN/m. The notations are the same as in Figure 6.

surface tension with AAPD of 2.5%. Without consideration of surface tensions, the TraPPE-CG force field provides a relatively poorer prediction of the surface tensions with AAPD of 5.2%. The FE-12-6 parameters developed in this work yield good values with AAPD of 3.1%. The uncertainties of calculated surface tensions using CG models are less than 2.5 mN/m, which is approximately a half of that at the AA level.

The parameters for the rest pair interactions, C3E-C3M, C3M-C3M, C2E-C2E, C2E-C3E, and C2E-C3M, were derived by fitting the properties of pentane, heptane, octane, decane, nonane, and dodecane. The same procedure as explained above was used for these parametrizations. The combined parameters were derived using the VLE data, and then the energetic parameters were separated out using the HOV data. A total of 150 data points were used to fit the 20 parameters.

Comparisons of calculated VLE curves of these alkane molecules with experimental data are shown in Figure 8. Similar to hexane, both SDK and TraPPE-CG force fields overestimate the liquid densities and underestimate the vapor densities at high temperatures, and the deviations become larger as the temperature increases. The Martini force field was used for octane and dodecane only, but it was completely failed for the VLE calculations. It is clear that the simulation data obtained with the FE-12-6 parameters are in good agreement with the experimental data. Over a 300 K (from 275 to 600 K) temperature range, the AAPDs are 0.68% for liquid densities and 6.20% for vapor densities. The data for pentane are worse than others, which is likely due to the simplicity in the intramolecular functions.[22]

The HOV results are shown in Figure 9. The uncertainties in calculated HOVs are lower than 0.2 kJ/mol. Similar to the case of hexane, with entropic contributions, SDK, and TraPPE-CG models underestimate the HOVs over the entire range of temperatures. We note that the Martini force field yields similar results as SDK and TraPPE-CG force fields. By separating the entropic contribution out, we obtained excellent prediction of HOVs with AAPDs of 1.5%.

The calculated saturated vapor pressures, liquid densities, and surface tensions of pentane, hexane, heptane, octane, nonane, decane, and dodecane at 1 atm are shown in Figure 10 (a-c). The simulation data obtained with the FE-12-6 parameters are in good agreement with the experimental values for these molecules. The AAPDs of vapor pressures, liquid densities, surface tensions, and vapor pressures are 6.5%, 0.6%, 3.3%, and 5.5% respectively. The predictions are consistent crossing different molecules, properties, and temperatures. The results are compared with those predicted using TraPPE-CG, SDK, and Martini CG models, which are either failed or not accurate in these predictions.

From the VLE curves, the critical temperatures and critical densities were computed, and the results are given in Table 2. For the critical temperatures, the differences between the simulated and experimental values are more than 10 K for pentane, heptane, and decane, and the differences are less than 5 K for hexane, octane, nonane, and dodecane. For comparison, the deviations obtained using the TraPPE-CG force field for hexane, nonane, and dodecane are 18, 19, and 9 K, respectively.[22] The critical densities are overestimated for pentane, octane, nonane, and dodecane and underestimated for hexane, heptane, and decane. The largest deviation is 6.9% for nonane, and the smallest deviation is 0.4% for heptane. For other alkane liquids, the deviations in critical densities are lower than 3%. For comparison, the critical densities predicted using TraPPE-CG are an average error of 5.6%,[22] significantly larger errors were obtained using the SDK force field, and the prediction was failed using the Martini force field.

To validate the new parameters further we extended the predictions to molecules outside of the parametrization training set. Table 3 summarizes the calculated HOVs, densities, and surface tensions with experimental data for comparison for larger alkane molecules. Although these molecules are not included in the training set, the predictions are satisfactory. The AAPDs are 2.0%, 0.4%, and 3.5% for HOVs, densities, and surface tensions, respectively.

DOI: 10.1021/acs.jctc.5b00573
J. Chem. Theory Comput. 2015, 11, 4760−4769

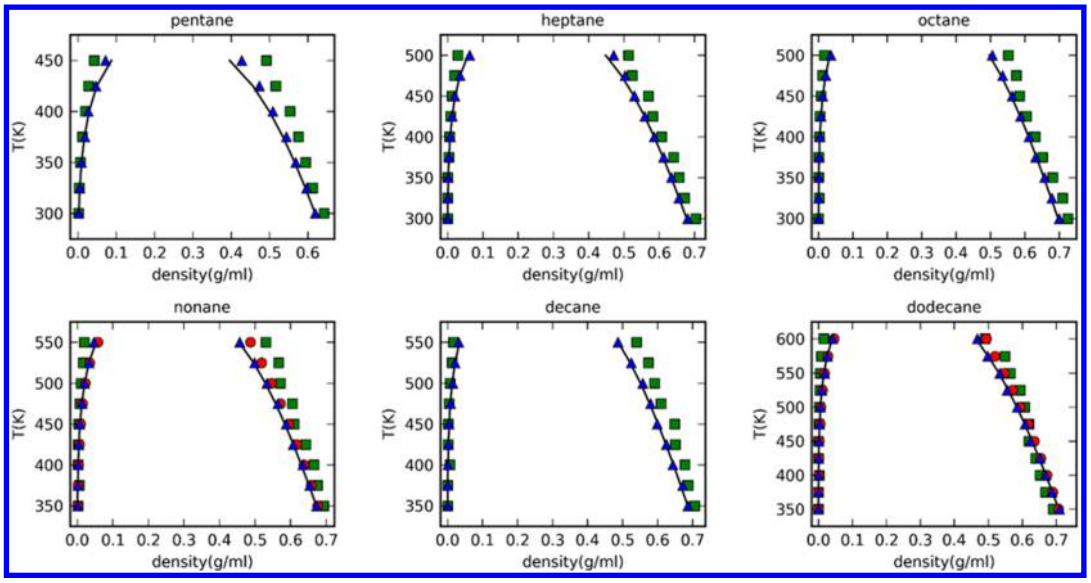

Figure 8. Comparison of the VLE curves for pentane, heptane, octane, nonane, decane, and dodecane. The notations are the same as in Figure 6.

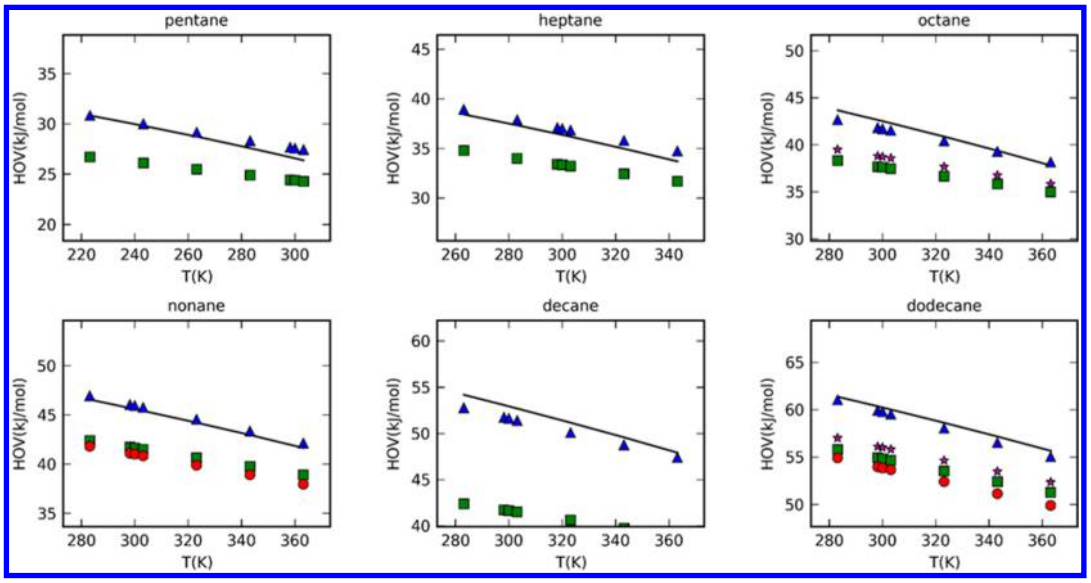

Figure 9. Comparison of HOVs for pentane, heptane, octane, nonane, decane, and dodecane at different temperature. The notations are experiment (solid line), SDK/FE-12-6 (blue triangle), TraPPE-CG (red cycle), SDK (green square), and Martini (purple star). The calculated uncertainties are lower than 0.2 kJ/mol.

The optimized FE-12-6 parameters are listed in Table 4. Despite the fact that these parameters are empirically derived, a general trend consisting with the degree of coarse-graining is observed. The order of atomic complexity represented by the beads is C3E > C3M > C2E. The same order is reflected in the radii parameters ($\sigma_{i,j}$), the energy parameters ($\varepsilon_{i,j}^{U}$), and the entropic parameters ($\delta\varepsilon$). The more atoms are included in the pairwise beads, the larger absolute values of these parameters are. The negative values in the entropic parameters are consistent with the analysis of PMFs presented above (Figure 1).

Finally, we tested whether or not a combination law can be used to calculate parameters of unlike bead-pairs (C2E-C3M, C2E-C3E, and C3E-C3M). Two combination laws, Lorentz–Berthelot[49] (LB) and the sixth-order,[52] were investigated. The results are summarized in Table 5. For the radii, energetic and residual entropic parameters ($\sigma_{i,j}$, $\varepsilon_{i,j}^{U}$, ε_{0}^{S}), both combination laws yield values scattering around the optimized parameters. The deviations can be attributed to the uncertainties in the empirical parametrizations. However, for the temperature-correction entropic parameter ($\delta\varepsilon$), both combination laws produce values systematically larger than those optimized, which indicates a new type of combination law is required for this term. Further study is needed because a very large amount of data is required to establish an empirical combination law.

V. CONCLUSIONS

In summary, based on an analysis of PMFs and PE calculated for propane dimers, we proposed a new FE-12-6 function with energetic and entropic parameters separated explicitly to describe the nonbond VDW interactions in CGFF. Although FE-12-6 cannot fit the PMF curves well, a cancellation of reduced radii and strong repulsion makes the function a good approximation. The FE-12-6 parameters were mainly derived

DOI: 10.1021/acs.jctc.5b00573
J. Chem. Theory Comput. 2015, 11, 4760–4769

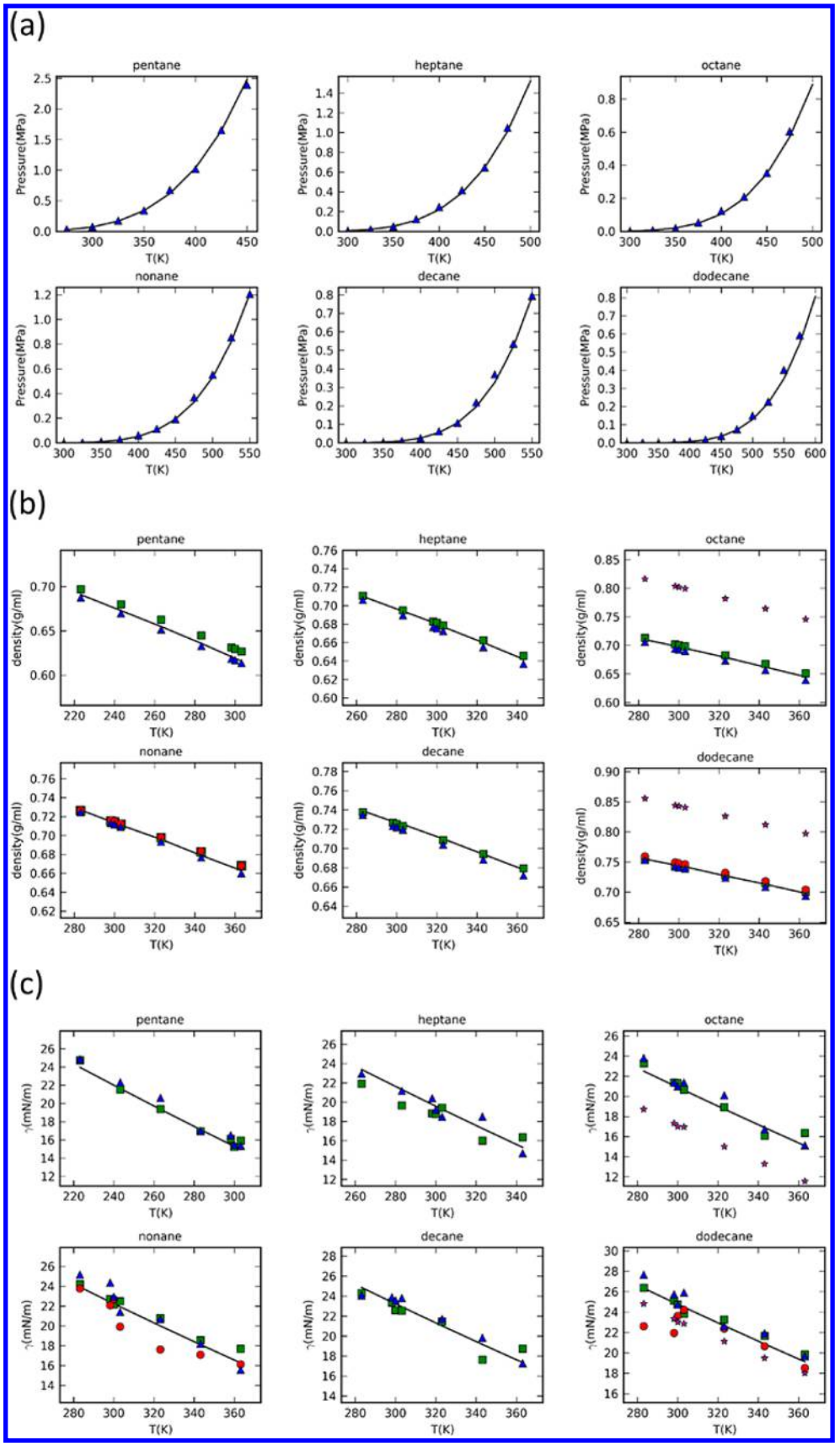

Figure 10. Comparison of (a) saturated vapor pressures, (b) liquid densities, and (c) surface tensions for pentane, heptane, octane, nonane, decane, and dodecane at different temperatures. The uncertainties of calculated pressure, density, and surface tension values are lower than 0.3 MPa, 0.0002 g/mL, and 2.5 mN/m, respectively. The notations are the same as in Figure 9.

DOI: 10.1021/acs.jctc.5b00573
J. Chem. Theory Comput. 2015, 11, 4760−4769

Table 2. Comparison of the Experimental and Calculated Critical Temperatures and Critical Densities of Alkane Molecules

	T_c (K)		ρ_c(g/mL)	
	expt	calc	expt	calc
pentane	469.70	496.91	0.232	0.236
hexane	507.82	503.38	0.233	0.215
heptane	540.13	553.75	0.232	0.232
octane	569.62	568.00	0.235	0.242
nonane	594.55	590.08	0.232	0.248
decane	617.70	642.18	0.233	0.228
dodecane	658.10	662.00	0.227	0.228

Table 3. Comparison of the Experimental and Calculated HOVs, Densities and Surface Tensions of Larger Alkane Liquids at 1 atm

	HOV(kJ/mol)		ρ (g/mL)		γ (mN/m)	
	expt	simu[c]	expt	simu[d]	expt	simu
tridecane[a]	66.3	66.0	0.753	0.749	25.38	23.9 ± 1.0
tetradecane[a]	71.2	70.0	0.757	0.756	25.98	24.7 ± 1.9
pentadecane[a]	75.9	74.6	0.764	0.762	26.51	26.3 ± 1.0
hexadecane[a]	77.0	79.1	0.769	0.765	26.92	25.8 ± 1.4
heptadecane[b]	79.6	81.9	0.759	0.756	25.61	24.2 ± 1.3
octadecane[b]	83.0	85.6	0.763	0.760	26.06	25.7 ± 1.2
nondecane[b]	89.7	90.7	0.767	0.762	26.37	25.1 ± 1.8
icosane[b]	92.2	94.6	0.770	0.766	26.77	26.6 ± 1.6

[a]Simulated at 300 K. [b]Simulated at 320 K. [c]The uncertainties are lower than 0.2 kJ/mol. [d]The uncertainties are lower than 0.0002 g/mL.

Table 4. Optimized FE-12-6 Parameters

	σ (Å)	ε^U (kJ/mol)	ε_0^S (kJ/mol)	$\delta\varepsilon^S$ (J/mol·K)
C2E-C2E	4.255	1.7573	−0.2081	−0.0732
C2E-C3M	4.373	2.0502	−0.2039	−0.0874
C2E-C3E	4.468	2.2175	−0.2998	−0.1862
C3M-C3M	4.518	2.2594	−0.1574	−0.2435
C3M-C3E	4.565	2.3598	−0.1274	−0.2586
C3E-C3E	4.615	2.6359	−0.1977	−0.5460

using the VLE data, and then the energetic parameters were separated from the entropic parameters using the HOV data. It is found that the radii parameters can be treated as temperature independent in a wide range (<200 K) of temperature, thus four (4) adjustable parameters are sufficient for each pairwise interaction. The FE-12-6 parameters are well transferrable for all alkane molecules including those outside of the training set, at different temperatures and for calculated various properties including VLE, HOV, density, vapor pressure, critical point, and surface tension. The good transferability is due to a clear representation of the free energy contribution in the functional form and well determined parameters based on high data/parameter ratio. We expect the force field can be used for predicting properties beyond those considered in this work. Although this work is limited to nonpolar molecules, the principle of representing free energy contribution holds for polar and ionic molecules. The challenge is to find suitable functional forms.

Table 5. Comparison the Optimized Parameters with Parameters Calculated Using Combination Laws for Unlike Bead Pairs

parameter	Comb. laws	C2E-C3M	C2E-C3E	C3E-C3M
σ (Å)				
	opt[a]	4.373	4.468	4.565
	LB[b]	4.386	4.435	4.567
	6th-order[c]	4.396	4.453	4.568
ε^U (kJ/mol)				
	opt	2.0502	2.2175	2.3598
	LB	1.9926	2.1522	2.4404
	6th-order	1.9608	2.0900	2.4354
ε_0^S (kJ/mol)				
	opt	−0.2039	−0.2998	−0.1274
	LB	−0.1808	−0.2028	−0.1764
	6th-order	−0.1779	−0.1970	−0.1759
$\delta\varepsilon^S$ (J/mol·K)				
	opt	−0.0874	−0.1862	−0.2586
	LB	−0.1336	−0.1999	−0.3646
	6th-order	−0.1314	−0.1941	−0.3639

[a]Optimized parameters taken from Table 4. [b]$\sigma_{ij} = (\sigma_{ij} + \sigma_{jj})/2$, $\varepsilon_{ij}^U = (\varepsilon_{ii}^U \varepsilon_{jj}^U)^{1/2}$, $x_{ij} = -(x_{ii}x_{jj})^{1/2}$ (x is ε_0^S or $\delta\varepsilon$). [c]$\sigma_{ij} = (((\sigma_{ii})^6 + (\sigma_{jj})^6)/2))^{1/6}$, $\varepsilon_{ij}^U = 2(\varepsilon_{ii}^U \varepsilon_{jj}^U)^{1/2}(((\sigma_{ii})^3 \cdot (\sigma_{jj})^3)/((\sigma_{ii})^6 + (\sigma_{jj})^6)))$, $x_{ij} = -(x_{ii}x_{jj})^{1/2}(((\sigma_{ii})^3 \cdot (\sigma_{jj})^3)/((\sigma_{ii})^6 + (\sigma_{jj})^6)))$.

■ ASSOCIATED CONTENT

Supporting Information

The Supporting Information is available free of charge on the ACS Publications website at DOI: 10.1021/acs.jctc.5b00573.

SDK model for linear alkanes; fitting results to propane dimer PMF curves by Buckingham and LJ-4-6 functions; tables listing the numerical data for the vapor−liquid coexistence curves, HOVs, densities, and surface tensions for alkane molecules (PDF)

■ AUTHOR INFORMATION

Corresponding Author

*E-mail: huaisun@sjtu.edu.cn.

Notes

The authors declare no competing financial interest.

■ ACKNOWLEDGMENTS

This work was partially funded by the National Natural Science Foundation of China (Nos. 21173146, 21473112, and 21403138) and the National Basic Research Program (No. 2014CB239702), and the computational resources are supported by the High Performance Computing (HPC) Center of Shanghai Jiao Tong University.

■ REFERENCES

(1) Voth, G. A. *Coarse-graining of condensed phase and biomolecular systems*; CRC Press: Boca Raton, FL, 2008.

(2) Riniker, S.; Allison, J. R.; van Gunsteren, W. F. On developing coarse-grained models for biomolecular simulation: a review. *Phys. Chem. Chem. Phys.* **2012**, *14*, 12423−12430.

(3) Brini, E.; Algaer, E. A.; Ganguly, P.; Li, C.; Rodríguez-Ropero, F.; van der Vegt, N. F. A. Systematic coarse-graining methods for soft matter simulations − a review. *Soft Matter* **2013**, *9*, 2108−2119.

(4) Noid, W. Systematic methods for structurally consistent coarse-grained models. In *Biomolecular Simulations*; Springer: 2013; pp 487−531.

DOI: 10.1021/acs.jctc.5b00573
J. Chem. Theory Comput. 2015, 11, 4760−4769

(5) Noid, W. Perspective: Coarse-grained models for biomolecular systems. *J. Chem. Phys.* **2013**, *139*, 090901.
(6) Li, Y.; Abberton, B. C.; Kröger, M.; Liu, W. K. Challenges in multiscale modeling of polymer dynamics. *Polymers* **2013**, *5*, 751−832.
(7) Ercolessi, F.; Adams, J. B. Interatomic potentials from first-principles calculations: the force-matching method. *Europhys. Lett.* **1994**, *26*, 583.
(8) Lyubartsev, A. P.; Laaksonen, A. Calculation of effective interaction potentials from radial distribution functions: A reverse Monte Carlo approach. *Phys. Rev. E: Stat. Phys., Plasmas, Fluids, Relat. Interdiscip. Top.* **1995**, *52*, 3730.
(9) Reith, D.; Pütz, M.; Müller-Plathe, F. Deriving effective mesoscale potentials from atomistic simulations. *J. Comput. Chem.* **2003**, *24*, 1624−1636.
(10) Izvekov, S.; Voth, G. A. A multiscale coarse-graining method for biomolecular systems. *J. Phys. Chem. B* **2005**, *109*, 2469−2473.
(11) Harmandaris, V.; Adhikari, N.; Van der Vegt, N.; Kremer, K. Hierarchical modeling of polystyrene: From atomistic to coarse-grained simulations. *Macromolecules* **2006**, *39*, 6708−6719.
(12) Shell, M. S. The relative entropy is fundamental to multiscale and inverse thermodynamic problems. *J. Chem. Phys.* **2008**, *129*, 144108.
(13) Mullinax, J. W.; Noid, W. G. A Generalized-Yvon−Born−Green Theory for Determining Coarse-Grained Interaction Potentials. *J. Phys. Chem. C* **2010**, *114*, 5661−5674.
(14) Wang, Y.; Noid, W.; Liu, P.; Voth, G. A. Effective force coarse-graining. *Phys. Chem. Chem. Phys.* **2009**, *11*, 2002−2015.
(15) Brini, E.; Marcon, V.; van der Vegt, N. F. Conditional reversible work method for molecular coarse graining applications. *Phys. Chem. Chem. Phys.* **2011**, *13*, 10468−10474.
(16) Brini, E.; van der Vegt, N. Chemically transferable coarse-grained potentials from conditional reversible work calculations. *J. Chem. Phys.* **2012**, *137*, 154113.
(17) Ganguly, P.; Mukherji, D.; Junghans, C.; van der Vegt, N. F. Kirkwood-Buff coarse-grained force fields for aqueous solutions. *J. Chem. Theory Comput.* **2012**, *8*, 1802−1807.
(18) Marrink, S. J.; Risselada, H. J.; Yefimov, S.; Tieleman, D. P.; de Vries, A. H. The MARTINI force field: coarse grained model for biomolecular simulations. *J. Phys. Chem. B* **2007**, *111*, 7812−7824.
(19) Shinoda, W.; Devane, R.; Klein, M. Multi-property fitting and parameterization of a coarse grained model for aqueous surfactants. *Mol. Simul.* **2007**, *33*, 27−36.
(20) Shinoda, W.; DeVane, R.; Klein, M. L. Zwitterionic Lipid Assemblies: Molecular Dynamics Studies of Monolayers, Bilayers, and Vesicles Using a New Coarse Grain Force Field. *J. Phys. Chem. B* **2010**, *114*, 6836−6849.
(21) Chiu, S.-W.; Scott, H. L.; Jakobsson, E. A Coarse-Grained Model Based on Morse Potential for Water and n-Alkanes. *J. Chem. Theory Comput.* **2010**, *6*, 851−863.
(22) Maerzke, K. A.; Siepmann, J. I. Transferable Potentials for Phase Equilibria−Coarse-Grain Description for Linear Alkanes. *J. Phys. Chem. B* **2011**, *115*, 3452−3465.
(23) Avendaño, C.; Lafitte, T.; Galindo, A.; Adjiman, C. S.; Jackson, G.; Müller, E. A. SAFT-γ Force Field for the Simulation of Molecular Fluids. 1. A Single-Site Coarse Grained Model of Carbon Dioxide. *J. Phys. Chem. B* **2011**, *115*, 11154−11169.
(24) Avendano, C.; Lafitte, T.; Adjiman, C. S.; Galindo, A.; Muller, E. A.; Jackson, G. SAFT-γ Force Field for the Simulation of Molecular Fluids: 2. Coarse-Grained Models of Greenhouse Gases, Refrigerants, and Long Alkanes. *J. Phys. Chem. B* **2013**, *117*, 2717−2733.
(25) Lafitte, T.; Avendaño, C.; Papaioannou, V.; Galindo, A.; Adjiman, C. S.; Jackson, G.; Müller, E. A. SAFT-γ force field for the simulation of molecular fluids: 3. Coarse-grained models of benzene and hetero-group models of n-decylbenzene. *Mol. Phys.* **2012**, *110*, 1189−1203.
(26) Lobanova, O.; Avendaño, C.; Lafitte, T.; Müller, E. A.; Jackson, G. SAFT-γ force field for the simulation of molecular fluids: 4. A single-site coarse-grained model of water applicable over a wide temperature range. *Mol. Phys.* **2015**, *113*, 1228−1249.
(27) Carbone, P.; Varzaneh, H. A. K.; Chen, X.; Müller-Plathe, F. Transferability of coarse-grained force fields: The polymer case. *J. Chem. Phys.* **2008**, *128*, 064904.
(28) Qian, H.-J.; Carbone, P.; Chen, X.; Karimi-Varzaneh, H. A.; Liew, C. C.; Müller-Plathe, F. Temperature-transferable coarse-grained potentials for ethylbenzene, polystyrene, and their mixtures. *Macromolecules* **2008**, *41*, 9919−9929.
(29) Farah, K.; Fogarty, A. C.; Böhm, M. C.; Müller-Plathe, F. Temperature dependence of coarse-grained potentials for liquid hexane. *Phys. Chem. Chem. Phys.* **2011**, *13*, 2894−2902.
(30) Krishna, V.; Noid, W. G.; Voth, G. A. The multiscale coarse-graining method. IV. Transferring coarse-grained potentials between temperatures. *J. Chem. Phys.* **2009**, *131*, 024103.
(31) Villa, A.; Peter, C.; van der Vegt, N. F. Transferability of nonbonded interaction potentials for coarse-grained simulations: Benzene in water. *J. Chem. Theory Comput.* **2010**, *6*, 2434−2444.
(32) Fritz, D.; Harmandaris, V. A.; Kremer, K.; van der Vegt, N. F. Coarse-grained polymer melts based on isolated atomistic chains: simulation of polystyrene of different tacticities. *Macromolecules* **2009**, *42*, 7579−7588.
(33) Das, A.; Lu, L.; Andersen, H. C.; Voth, G. A. The multiscale coarse-graining method. X. Improved algorithms for constructing coarse-grained potentials for molecular systems. *J. Chem. Phys.* **2012**, *136*, 194115.
(34) Mie, G. Zur kinetischen Theorie der einatomigen Körper. *Ann. Phys.* **1903**, *316*, 657−697.
(35) Jorgensen, W. L.; Maxwell, D. S.; Tirado-Rives, J. Development and Testing of the OPLS All-Atom Force Field on Conformational Energetics and Properties of Organic Liquids. *J. Am. Chem. Soc.* **1996**, *118*, 11225−11236.
(36) Martin, M. G.; Siepmann, J. I. Transferable Potentials for Phase Equilibria. 1. United-Atom Description of n-Alkanes. *J. Phys. Chem. B* **1998**, *102*, 2569−2577.
(37) Sun, H. COMPASS: An ab Initio Force-Field Optimized for Condensed-Phase ApplicationsOverview with Details on Alkane and Benzene Compounds. *J. Phys. Chem. B* **1998**, *102*, 7338−7364.
(38) Lu, L.; Voth, G. A. The multiscale coarse-graining method. VII. Free energy decomposition of coarse-grained effective potentials. *J. Chem. Phys.* **2011**, *134*, 224107.
(39) Izvekov, S. Towards an understanding of many-particle effects in hydrophobic association in methane solutions. *J. Chem. Phys.* **2011**, *134*, 034104.
(40) Cao, Z.; Dama, J. F.; Lu, L.; Voth, G. A. Solvent Free Ionic Solution Models from Multiscale Coarse-Graining. *J. Chem. Theory Comput.* **2013**, *9*, 172−178.
(41) Torrie, G. M.; Valleau, J. P. Monte Carlo free energy estimates using non-Boltzmann sampling: Application to the sub-critical Lennard-Jones fluid. *Chem. Phys. Lett.* **1974**, *28*, 578−581.
(42) Kumar, S.; Rosenberg, J. M.; Bouzida, D.; Swendsen, R. H.; Kollman, P. A. The weighted histogram analysis method for free-energy calculations on biomolecules. I. The method. *J. Comput. Chem.* **1992**, *13*, 1011−1021.
(43) Hub, J. S.; De Groot, B. L.; Van Der Spoel, D. g_wham · A Free Weighted Histogram Analysis Implementation Including Robust Error and Autocorrelation Estimates. *J. Chem. Theory Comput.* **2010**, *6*, 3713−3720.
(44) Hess, B.; Kutzner, C.; Van Der Spoel, D.; Lindahl, E. GROMACS 4: algorithms for highly efficient, load-balanced, and scalable molecular simulation. *J. Chem. Theory Comput.* **2008**, *4*, 435−447.
(45) Panagiotopoulos, A. Z. Direct determination of phase coexistence properties of fluids by Monte Carlo simulation in a new ensemble. *Mol. Phys.* **1987**, *61*, 813−826.
(46) Martin, M. G. MCCCS Towhee: a tool for Monte Carlo molecular simulation. *Mol. Simul.* **2013**, *39*, 1212−1222.
(47) Martínez, L.; Andrade, R.; Birgin, E. G.; Martínez, J. M. PACKMOL: a package for building initial configurations for molecular dynamics simulations. *J. Comput. Chem.* **2009**, *30*, 2157−2164.

DOI: 10.1021/acs.jctc.5b00573
J. Chem. Theory Comput. 2015, 11, 4760−4769

(48) Plimpton, S. Fast parallel algorithms for short-range molecular dynamics. *J. Comput. Phys.* **1995**, *117*, 1−19.
(49) Allen, M. P.; Tildesley, D. J. *Computer simulation of liquids*; Oxford University Press: New York, 1987.
(50) Lafitte, T.; Bessieres, D.; Piñeiro, M. M.; Daridon, J.-L. Simultaneous estimation of phase behavior and second-derivative properties using the statistical associating fluid theory with variable range approach. *J. Chem. Phys.* **2006**, *124*, 024509.
(51) Potoff, J. J.; Bernard-Brunel, D. A. Mie Potentials for Phase Equilibria Calculations: Application to Alkanes and Perfluoroalkanes. *J. Phys. Chem. B* **2009**, *113*, 14725−14731.
(52) Waldman, M.; Hagler, A. T. New combining rules for rare gas van der waals parameters. *J. Comput. Chem.* **1993**, *14*, 1077−1084.

DOI: 10.1021/acs.jctc.5b00573
J. Chem. Theory Comput. 2015, 11, 4760−4769